NASA Technical Paper 3054

November 1990

Thermal-Distortion Analysis of a Spacecraft Box Truss in Geostationary Orbit

Patrick A. Cosgrove,
Jeffery T. Farmer,
and Lawrence F. Rowell

NASA Technical Paper 3054

1990

Thermal-Distortion Analysis of a Spacecraft Box Truss in Geostationary Orbit

Patrick A. Cosgrove
Lockheed Engineering & Sciences Company
Hampton, Virginia

Jeffery T. Farmer and Lawrence F. Rowell
Langley Research Center
Hampton, Virginia

National Aeronautics and Space Administration
Office of Management
Scientific and Technical Information Division

Summary

The Mission to Planet Earth program may enlist the use of geostationary platforms to support Earth-science monitoring instruments. The strongback for a proposed geostationary platform is a deployable box truss that supports two large-diameter passive microwave radiometers (PMR's) and several other science instruments. A study was made to estimate the north-south and east-west pointing errors at the mounting locations of the two PMR's due to on-orbit thermal distortions of the main truss. The baseline configuration for the main truss was modeled as untreated graphite/epoxy composite truss members and end fittings to illustrate typical thermal behaviors for structures of this type.

Analytical results of the baseline configuration indicated that the east-west pointing error greatly exceeded the required limits. Primary origins of the pointing errors were identified, and methods for their reduction were addressed. Thermal performance enhancements to the truss structure were modeled and analyzed, including state-of-the-art surface coatings and insulation techniques. Comparisons of the thermal enhancements to the baseline were made. Results demonstrated that using a thermal-enclosure insulating technique reduced external heat fluxes and distributed those heat fluxes more evenly throughout the structure, sufficiently reducing the pointing errors induced by thermal distortions to satisfy pointing accuracy requirements of the PMR's.

Introduction

The proposed Mission to Planet Earth program will employ a combination of low Earth orbit (LEO) and geostationary Earth orbit (GEO) spacecraft as Earth-science instrument platforms. The mission of the program is to monitor global changes in the Earth's hydrological, biogeochemical, and climatological cycles. At geostationary altitude, the coordination of a small number of spacecraft will facilitate continuous coverage of a large percentage of the Earth's land, ocean, and atmospheric area, as well as provide high temporal coverage and reduce the number of LEO spacecraft required to obtain comparable coverage. However, placing the observation platforms at geostationary altitudes places high demands on a broad range of current technologies. Particularly, advances in technology will be required to meet high pointing accuracy requirements and provide the pointing and position knowledge required intrinsically at GEO.

In order to quantify the needs for such advanced technology, the NASA Langley Research Center (LaRC) is studying the performance of a proposed geostationary platform concept (fig. 1). This concept consists of a housekeeping module and a payload module, two large-diameter passive microwave radiometers (PMR's), and a number of other instruments mounted on a supporting box truss structure. The two passive microwave radiometers, one with a 15-m diameter and one with a 7.5-m diameter, are deployed on opposite ends of the spacecraft. The housekeeping and payload modules function as the main instrument bus and support several of the highest precision instruments on the spacecraft.

Because of high-precision pointing requirements for many of the instruments, the calculation of spacecraft mechanical distortions is vital to spacecraft design and performance. Structural distortions arise from both dynamic and thermal disturbances. The structural characteristics of this platform, along with the finite-element model used in the structural analysis, have been documented in presently unpublished data by L. F. Rowell of LaRC and G. D. Qualls of Flight Mechanics and Controls. The analysis of the large 15-m PMR is presented in reference 1. Examples of dynamic disturbances include torques induced by thruster firings and movements of solar arrays or articulating components of the instruments themselves. The dynamic behavior of this platform, when subjected to representative on-orbit disturbances, was assessed by Rowell and Qualls and was shown to meet estimated pointing requirements. However, depending upon spacecraft materials and design, distortions due to the thermal gradients across the structure induced by orbital heating and cooling are severe relative to those due to the vibrational environment, and therefore they must be quantitatively analyzed. Thermal analysis of the 7.5-m radiometer has been presented in reference 2, and the thermal distortion analysis of the supporting box truss of the platform is reported herein.

The finite-element model described by Rowell and Qualls is converted to a finite-difference model for thermal analysis to determine on-orbit temperature profiles. Temperature variations are calculated for each discrete thermal node for two different geostationary orbits, specifically an equinox orbit and a solstice orbit. These temperature results are used as input loads to estimate resulting structural deformations. Deformations resulting in both bending and torsion of the box truss are reported in terms of pointing errors at the mounting locations of the two PMR's. Any resulting deficiencies in performance indicated by excessive pointing errors demonstrate a need for alternate thermal designs. The baseline configuration consists of uncoated graphite/epoxy composite truss members. Alternatives to the baseline configuration include truss-member surface coatings,

multilayer insulation, and a truss-enclosing thermal blanket. A comparison of the performance of alternative thermal design concepts with that of the baseline configuration is presented.

Spacecraft Concept

Many concepts for a geostationary platform have been proposed in studies performed for NASA by the General Electric Astro-Space Division, Lockheed Missiles & Space Company, Ford Aerospace Corporation, and others. The concept selected for this analysis resulted from a Ford Aerospace study completed in 1987, and it is shown in figure 1. It is representative of the large Earth-science platforms anticipated to support the high-resolution instruments required to make global-change measurements. The fact that the strongback is a large truss, rather than a rigid panel structure, and can be deployed or erected on-orbit is also representative of scenarios being proposed for the assembly of large, multidisciplinary platforms at Space Station *Freedom*. This spacecraft, serving as a science instrument platform, must satisfy pointing criteria for 18 distinct science instruments with pointing requirements ranging from 1 to 360 arcseconds (arcsec). The main box truss (developed by A. von Roos and J. M. Hedgepeth of Astro Aerospace Corporation) serves as the strongback for the GEO spacecraft and is constructed of graphite/epoxy composite tubes designed as a fully deployable, packaged truss. (See sketch A.) The lacing pattern of the truss is specifically designed to make the structure deployable. The tubes form seven cubic 3.0-m bays and are attached to the truss nodes by graphite end fittings.

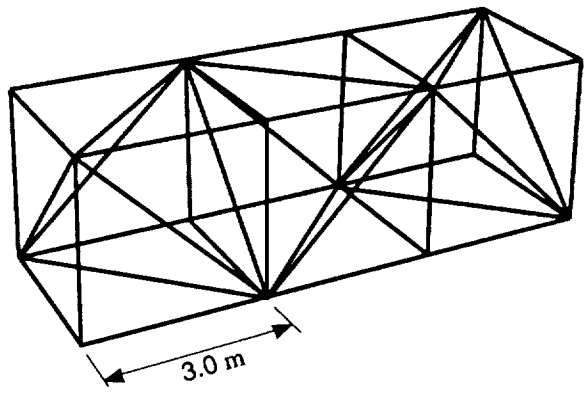

Sketch A

The housekeeping module accommodates most of the spacecraft subsystem components including the sensors and actuators for attitude control. The pointing and alignment knowledge and control are implemented at this rigidized point of the spacecraft. For this reason, the payload module accommodates those science instruments requiring the highest pointing precision. These modules are reinforced with graphite honeycomb panels to provide added stiffness. Since the sensors and actuators for pointing control are located in the housekeeping and payload (H/P) modules, the support structure for the H/P modules must be designed to eliminate transmission of mechanical distortions from the spacecraft to the modules. Therefore, these modules have a very rigid construction relative to the box truss.

The 15-m PMR is mounted at the end of the bus truss nearest the H/P modules, whereas the 7.5-m PMR is at the farthest end in order to balance the solar pressure torques that each PMR encounters. An adjustable solar sail is also used to provide adaptability to seasonal variations in solar pressure torque. Other science instruments, mounted at various locations along the main truss, have stringent pointing requirements that dictate a stiff supporting structure. Also, accommodating the fields of view of individual instrument sensors and radiators suggests a complex system integration and governs the overall configuration layout.

Platform Thermal-Structural Model

The structural model of the GEO platform is a finite-element model (developed by Rowell and Qualls) that is generated with I-DEAS software. (See the appendix and ref. 3.) The finite-element model is converted to a finite-difference model using the Thermal Model Generator (TMG). (See the appendix and ref. 4.) Because this study addresses the pointing error inherent in the structure of the spacecraft main box truss, the portion of the complete platform model required for this study includes only the components that make up the main bus truss (fig. 2). The "R's" in figure 2 (see views 1 and 2) designate the rigid bar elements that connect the PMR's to the platform. The graphite/epoxy composite tubes that are the truss longerons, batons, and diagonals are modeled as two-node isotropic linear beam elements. The graphite end fittings and truss node regions are modeled as single-node, isotropic lumped mass elements.

Modeling of the radiative exchanges between the individual payloads and the shadowing effects of the individual science payloads on the box truss have not been considered. Although the thermal effects of the H/P modules have not been modeled for this analysis, their contribution to the structural stiffness of the platform is considered in the formulation of the analysis boundary conditions. The assumed boundary conditions define zero translations and rotations at the four nodes of attachment between the H/P modules and the bus truss.

Therefore, any nodal translations or rotations encountered at various locations along the truss are calculated relative to these boundary-condition locations using the I-DEAS model solution analysis package. (See the appendix and ref. 5.) The rotation of any node is considered analogous to the pointing error for any instrument mounted at that node. Therefore, pointing errors at any node location of the model are determined relative to the H/P modules. Thermophysical properties used in the baseline analysis are taken from the analysis presented in reference 2 and are given in table I. Note that all properties are assumed to be constant with respect to temperature and are representative of beginning-of-life values.

Table I. Thermophysical Properties of Finite-Element Model

Linear beam characteristics:	
Diameter, mm	51
Thickness, mm	1.6
Average length, m	3.0
Material properties (uncoated P75 graphite/thermoplastic):	
Young's modulus, N/m^2	2.7×10^{11}
Mass density, kg/m^3	1690
Coefficient of thermal expansion (CTE), m/m-K	0.5×10^{-6}
Thermal conductivity, W/m-K	76
Specific heat, J/kg-K	850
Surface properties:	
Solar absorptivity (α)	0.9
Thermal emissivity (ϵ)	0.8
Lumped mass characteristics (end fittings/truss node region):	
Mass, kg	7.0
Rigid bar characteristics:	
Infinite stiffness	
Nonthermal element	

The use of untreated or unprotected graphite in a geostationary spacecraft design may not be practical because of material lifetime limitations and inadequate thermal performance. However, the use of this configuration serves as a baseline against which all performance-enhancing treatments or technologies can be compared.

The performance of the box truss model just described is measured in terms of east-west and north-south pointing errors at the two PMR mounting locations which correspond to nodal rotations about the model Y-axis and X-axis, respectively (fig. 2). The PMR mounting locations have been chosen because they are at the extreme ends of the truss, and it is anticipated that the pointing errors increase as the distance from the H/P modules increases. Relative to the rotations in the X- and Y-axes, the nodal rotations about the model Z-axis are not significant in terms of the spacecraft performance. The PMR's must achieve pointing accuracies within 36 arc-seconds (ref. 6) in the north-south and east-west directions to meet performance specifications.

It is important to note that this specified pointing requirement is the maximum allowable total of all pointing error contributors. Also, pointing errors for the PMR's are expressed as positive or negative errors. Positive pointing error is defined here as a clockwise rotation about an axis when the rotation is viewed from the origin with the viewer facing in the positive axis direction, and negative pointing error is a counterclockwise rotation. As expressed previously, structural distortions of the platform are induced by mechanical disturbances and vibrations as well as by thermal gradients within the structure. Therefore, the pointing errors induced by orbital thermal distortions represent only one part of the total, and discretion must be exercised in characterizing a particular thermal performance as meeting the pointing requirements.

Scope of Analyses

The intent of this study is to determine the effect of the geostationary orbit thermal environment on the pointing performance of the GEO platform in terms of thermally induced pointing errors at the extreme ends of the box truss. Thermal analyses provide temperature profiles of the truss as a function of time in orbit. These temperature profiles serve as the load sets for the linear static analyses, the results of which are nodal displacements and rotations.

Details of Thermal Analysis

The thermal environment of the GEO platform can be broken down into three components of influence: radiative heat fluxes from the Sun and Earth, radiative and conductive heat exchanges between elements of the platform, and radiative exchange between the platform and deep space. The view factor between thermal node A and thermal node B is defined as the fraction of the radiant energy flux that leaves A which is incident upon B. The solar absorptivity surface property for a thermal node determines the fraction of incident radiant energy flux that is absorbed, and the thermal or infrared emissivity determines the fraction of blackbody radiant energy flux that is emitted. Therefore, the radiative heat exchanges between the Sun, Earth, and/or deep space and the truss structure are calculated by

determining the orbital changes in view factors between them. Similarly, the radiative heat exchanges within the platform are calculated by determining the view factors between individual truss members. Calculations of these view factors and energy exchanges are performed by the TMG. (See the appendix and ref. 4.)

Increases or decreases in solar heating on individual truss members are caused by changes in their orientation relative to the Sun as the spacecraft orbits the Earth. The GEO orbit is an equatorial orbit (0° inclination) with a radius of 42 164 km and an orbital period equal to that of the Earth. In order to quantify the performance of the box truss with regard to orbital variations, this study considers both equinox and solstice orbits. Figure 3 shows the relative orientation of the spacecraft, Earth, and Sun at equinox and solstice orbits. In the equinox orbit, part of each orbit passes through the shadow cast by the Earth. The maximum eclipse time is approximately 72 minutes, occurring on both the spring equinox and the fall equinox. For approximately 22 days on each side of an equinox there are eclipses of shorter duration. During the remaining days, the spacecraft is in sunlight for the entire orbit. Over the course of a year, there are about 50 days with eclipse periods of more than 1 hour (ref. 7). As the spacecraft enters the Earth's shadow, temperatures fall and will subsequently rise upon exit from the shadow with the resumption of incident solar flux. Changes in element temperature in the box truss as it passes through the Earth's shadow lead to deformations and stresses due to thermal expansion and contraction.

Another shadowing effect occurs when truss members are shadowed by other truss members, as depicted in figure 4. Note that there are no diagonals shown in the figure for simplicity of illustration, and that diagonals have been included for the calculation of view factors. When one truss member shadows another, the shadowing member intercepts the incident collimated solar flux such that the shadowed member receives little or no solar flux, thus producing a thermal gradient in the structure. This internal shadowing is particularly acute in the equinox orbit when the longerons of the truss on the Sun's facing side shadow the longerons of the opposite side because of their coincident projected areas. Because this occurs over a large portion of the equinox orbit, there are long time periods with large temperature gradients between opposing sides of the truss, with resulting thermal distortions. In contrast, because of the introduction of an incident Sun angle of 23.5° with respect to the orbit plane, the internal shadowing of the box truss in the solstice orbit is very minimal.

Details of Structural Analysis

Element distortions resulting from thermal expansions and contractions are expressed in terms of nodal displacements and rotations. Because adjacent elements share common nodes, displacements and rotations in the structure may be additive from one element to its connecting elements. To perform the linear static analysis, boundary conditions in the form of a restrained set of nodes were necessary. The mounting location of the H/P modules was chosen as the location for these boundary conditions, such that the connecting nodes between the H/P modules and the spacecraft bus truss have their displacements and rotations restrained. The rigid bar elements that connect science instrument payloads to the truss are not thermal elements and, therefore, are not part of the matrix solution with regard to thermal distortions and stresses.

Results of Analysis

Baseline Configuration

Thermal characteristics. The surface properties used in the baseline configuration represent uncoated graphite/epoxy composite materials with high solar absorptivity ($\alpha = 0.9$) and emissivity ($\epsilon = 0.8$) for all truss members. High solar absorptivity corresponds to a high percentage of incident solar radiation being absorbed, and high emissivity corresponds to a high percentage of blackbody radiation being emitted. As stated previously, the orientation of truss members relative to the incident solar flux changes throughout the orbit, and therefore this configuration has wide swings in element heat fluxes. Because the temperature of a truss member is directly dependent on the net heat flux on its surface, there are corresponding wide swings in temperature as the spacecraft proceeds through its orbit. For the purpose of describing trends in thermal performance for the cases analyzed, the maximum, minimum, and average temperatures are specified. Note that for the purpose of calculating structural distortions and stresses, the predicted truss member temperatures have been used.

Equinox orbit: At equinox the minimum and maximum truss member temperatures for the baseline case are −172°C and 20°C, respectively, under transient conditions. Note that these temperatures are the extremes for the entire model over the entire orbit and refer simply to one particular truss member at one particular time in orbit. Figure 5 shows the average element temperature as a function of time in equinox orbit for the longerons on the Earth-facing side and on the anti-Earth-facing side.

Evident in figure 5 are the two following noteworthy characteristics.

The first characteristic is that internal shadowing of one side of the truss by the other occurs when the spacecraft approaches local noon and midnight. Figure 5 shows that as the spacecraft begins its orbit at 12:00 noon local time, the anti-Earth-facing side is directly exposed to incident solar flux. Internal shadowing eliminates direct solar heating of the Earth-facing side, thereby creating temperature differences as large as 170°C between the average temperatures on the Earth-facing and anti-Earth-facing sides at that time. Orbital progression through 6:00 pm brings the Earth-facing and anti-Earth-facing sides into an orientation where their projected areas view almost no solar flux, thereby greatly reducing the temperatures of the anti-Earth-facing longerons. Continuing past 6:00 pm toward local midnight, the Earth-facing longerons begin to receive direct solar flux and also begin to shadow the anti-Earth-facing longerons. This induces a comparable maximum temperature difference as seen earlier, except that the high- and low-temperature sides have been switched. The temperature profile is reversed after local 12:00 midnight, and thus the complete cycle is repeated every 24 hours.

The second characteristic evident in figure 5 is that the spacecraft is in the Earth's shadow for approximately 1 hour, roughly centered around 12:00 midnight local time. Immediately prior to that time only the Earth-facing side of the spacecraft is exposed to incident solar flux. The effect of the Earth's shadow is shown by the sharp drop and subsequent rise in the temperature curve of the Earth-facing longeron.

Solstice orbit: The solstice orbit exhibits an incident Sun angle of 23.5° with respect to the orbit plane. This has the effect of exposing to incident solar flux many of the truss members that had been shaded in the equinox orbit because of the internal shadowing. Having comparable solar fluxes on most truss members sharply reduces the temperature variations across the spacecraft. Figure 6 shows the average element temperatures as a function of time in a solstice orbit for the Earth-facing and anti-Earth-facing longerons. Here the temperature extremes span only about 80°C, less than half the 170°C span in the equinox case. Figure 6 also illustrates that when internal shadowing is reduced, the temperatures of the opposing truss members track each other and also have greatly reduced temperature differences between them. The temperature difference for this orbit is on the order of 10°C. Also note that there is no drop in the temperature curve around local midnight because the solstice orbit encounters no Earth shadow.

In the solstice orbit the minimum and maximum truss member temperatures for the baseline case are −148°C and 21°C, respectively. The maximum temperature is approximately the same as in the equinox orbit and corresponds to truss members that have complete exposure to the incident solar flux. The minimum temperature is considerably higher than that of the equinox orbit. Because the minimum temperature of a truss member is generally encountered when the member is shadowed from solar flux, the reduced occurrences and the duration of internal shadowing in the solstice orbit result in a higher minimum temperature.

Structural characteristics. The structural performance of the GEO platform has been analyzed in terms of the east-west and north-south pointing errors at the mounting locations of the two PMR's. For all cases analyzed, the assumed coefficient of thermal expansion (CTE) is 0.5×10^{-6} m/m-°C with an undistorted reference temperature of 22°C. Relative to this undistorted temperature, higher temperature members expand and lower temperature members contract. This causes distortions of the truss members relative to one another. East-west pointing error is caused by a temperature gradient between Earth-facing and anti-Earth-facing longerons. North-south pointing error is due to any uncompensated torsion effects that dissimilar expansions and contractions of the truss diagonals and batons impose on the spacecraft.

In addition to thermal distortions, orbital temperature fluctuations induce thermal stresses in the truss members. Therefore, analysis of the induced stresses was undertaken for both the equinox and solstice orbits. The results indicate that the induced stresses are far below the critical limits for both Euler buckling and tensile failure. Also, stresses are induced as the spacecraft enters and exits the Earth's shadow. Reference 8 suggests that characteristic stresses of this type are small, and the present analysis confirms this result.

Equinox orbit: Figure 7 shows the east-west pointing errors for the PMR's as a function of time in the equinox orbit. Quite prominent in the figure is that the magnitude of the pointing error of the 7.5-m PMR is much greater than that of the 15-m PMR. The east-west error of the 15-m PMR ranges from 25 to −15 arcseconds and that of the 7.5-m PMR ranges from 71 to −99 arcseconds. The reason for the excessive error (i.e., in excess of the specified limit of 36 arcseconds) of the 7.5-m PMR is that internal longeron shadowing creates large east-west

pointing errors, and this effect is additive from one bay to the next. Therefore, the combined pointing errors of the five bays that separate the 7.5-m PMR from the H/P modules exceed those of the one bay between the H/P module and the 15-m PMR.

Figure 7 also shows a sharp decrease in the magnitude of the pointing error around the orbit time of 11:30 pm when the spacecraft enters the Earth's shadow. During this time all truss elements have a common sink and temperatures approach uniformity. In addition, the sign of the east-west pointing errors changes around 6:00 pm and again at around 6:00 am. (Again, positive pointing error is defined as a clockwise rotation about an axis when the rotation is viewed from the origin with the viewer facing in the positive axis direction.) These two times indicate when the axis of travel of the platform is parallel with the collimated solar flux and define the point of the orbit where the truss switches Sun-facing sides. Consequently, the sides in contraction and expansion are switched, and therefore the rotation about the model Y-axis, analogous to east-west pointing error, reverses sign around 6:00 pm and again around 6:00 am.

For the equinox case, the north-south pointing error of the 15-m PMR ranges from 15 to -3 arcseconds, and that of the 7.5-m PMR ranges from -2 to -19 arcseconds. These pointing errors are well within the specified limit of 36 arcseconds. The lacing pattern of the truss is such that the torsion effect in one bay is offset with opposing torsion effects in an adjacent bay. As illustrated by the finite-element model in figure 2, there are five truss bays between the H/P module and the 7.5-m PMR and one truss bay between the H/P module and the 15-m PMR. Because of the uneven number of bays in each case and because the lacing pattern, chosen for deployability, causes adjacent bays to oppose each other in torsion, there are unopposed torsion effects manifested in north-south pointing errors that are comparable at each PMR. This effect was verified for the 7.5-m PMR by restraining the truss bay adjacent to the H/P module, thus canceling the torsion effects in that bay and resulting in a nearly zero net north-south pointing error for the 7.5-m PMR. Figure 8 shows the reduction in the north-south pointing error of the 7.5-m PMR when the structural model has additional restrained nodes in the bay adjacent to the H/P module bay.

There are various means by which the structure could conceivably be designed to yield balanced torsion effects, thus greatly reducing or eliminating the north-south pointing error. Having an even number of unrestrained bays would provide this balancing. Also, because the torsion effects are conveyed through the truss diagonals, altering the diagonal lacing pattern of the spacecraft would likely have significant effects on the north-south error. Each of these design choices may impart a potentially significant impact on other aspects of the total design, and such design changes would require careful examination.

Solstice orbit: As demonstrated in the previous section, the large temperature difference between the Earth-facing and anti-Earth-facing longerons in the equinox orbit is the primary cause for the east-west pointing error. Because the incident Sun angle in the solstice orbit reduces internal shadowing effects, no large temperature differences exist. Therefore, the east-west pointing errors are greatly reduced in the solstice orbit. Figure 9 shows the east-west pointing errors of the 15-m and 7.5-m PMR's as a function of time in the solstice orbit. The east-west pointing error of the 15-m PMR ranges from 6 to -2 arcseconds, and that of the 7.5-m PMR ranges from 0 to -9 arcseconds. Comparing the figures of equinox pointing error and solstice pointing error illustrates that the equinox orbit is far more severe and should be considered the worst-case orbital environment for this analysis.

As was the case in the equinox orbit, the north-south pointing error is caused by unbalanced torsion effects. The north-south pointing error of the 15-m PMR ranges from 2 to -17 arcseconds, and that of the 7.5-m PMR ranges from 14 to -8 arcseconds. Balancing the torsion effects of the diagonals and batons by restraining the adjacent bay, as discussed previously, resulted in the practical elimination of the north-south pointing errors.

Thermal Performance Enhancements

The excessive east-west pointing errors in the equinox orbit described above dictate that thermal performance enhancements of the spacecraft main bus truss are necessary. Several enhancements were analyzed and are summarized in table II. These include surface coatings, multilayer insulation (MLI), and a thermal enclosure of aluminized Du Pont Kapton. The capabilities of the performance enhancements to reduce moderate temperature gradients in the truss, thus reducing east-west pointing error under equinox orbital conditions, are compared. North-south pointing errors have also been examined for all the cases listed. Because the magnitude of the errors is within the specified limits and because of the previously discussed dependence of the error on the truss design (lacing pattern, number of bays, etc.), the north-south results will not be presented.

Surface coatings. In general, surface coatings are applied directly to graphite structural members

to protect them from various elements of the space environment in order to temper their thermal response and increase their lifetime. More specifically, for this analysis the intent is to adjust the ratio of solar absorptivity to emissivity (α/ϵ) so as to produce a favorable energy balance for the structure. The surface coatings used in this analysis consist of thin layers of etched aluminum. The different α/ϵ ratio of each coating is obtained by varying the control parameters of the etching process (ref. 9). Figure 10 shows the east-west pointing error of the 7.5-m and 15-m PMR's for the two surface-coated configurations superimposed on the results of the baseline configuration discussed previously.

Table II. Analysis Cases

Cases	Configuration	Thermal performance enhancement
1	Baseline	Truss members constructed of uncoated graphite with $\alpha/\epsilon = 0.9/0.8$
2	Low α/ϵ	Truss members constructed of surface-coated graphite with $\alpha/\epsilon = 0.3/0.65$
3	High α/ϵ	Truss members constructed of surface-coated graphite with $\alpha/\epsilon = 0.3/0.2$
4	MLI sleeving	Truss members individually wrapped with MLI with an effective α/ϵ of 0.05/0.05
5	First thermal blanket	Uncoated-graphite box truss wrapped in an aluminized Kapton blanket with an outside-surface α/ϵ of 0.3/0.2 and an inside-surface α/ϵ of 0.9/0.8
6	Final thermal blanket	Uncoated-graphite box truss wrapped in an aluminized Kapton blanket with an outside-surface α/ϵ of 0.3/0.65 and an inside-surface α/ϵ of 0.3/0.2

First coating: The first surface coating employed a low α/ϵ ratio of 0.3/0.65 which decreased the amount of solar radiation absorbed in the sunlit portions of the orbit and slightly decreased the amount of emitted radiation at lower temperatures. However, the decrease in emitted radiation was not great enough to offset the more substantial reduction in absorbed radiation. The result was that the overall heat balance was not greatly affected and the temperature gradient between opposing longerons remained quite large. Therefore, the overall effect on the pointing performance of the spacecraft was not substantial, and in the equinox orbit the calculated east-west pointing errors remained in excess of the specified limit of 36 arcseconds.

Second coating: The second surface coating employed a high α/ϵ ratio of 0.3/0.2 which further decreased the emitted thermal radiation from individual bus truss members to deep space, especially during shadowing, and also decreased the absorbed solar radiation incident on the truss members during their sunlit periods. Although the change in surface properties did slightly improve the pointing error of the PMR's around solar midnight, there was virtually no change at other points in the orbit.

The effectiveness of the baseline and the surface-coated configurations relative to one another varies with orbit position. Although neither of the coating concepts sufficiently lowers the error to within specified limits, the low-ratio coating has a slightly better performance. By maintaining cooler temperatures on those truss members exposed to direct solar radiation, the low-ratio coating reduces the temperature difference between opposing sides of the truss, thereby reducing the east-west pointing errors.

MLI sleeving. The third performance enhancement analyzed was a sleeving of MLI wrapped around individual truss members. By wrapping the individual truss members with MLI, the added thermal resistance serves as a radiative buffer between the orbital environment and the structure. The effective radiative properties of the truss members wrapped with MLI were assumed to have a solar absorptivity of 0.05 and an emissivity of 0.05. The lower solar absorptivity and emissivity significantly reduce the temperature gradients between the Earth-facing and anti-Earth-facing sides of the truss, thus reducing the pointing error by a proportionate amount. However, in the equinox orbit internal shadowing still occurs, which causes temperature differences between the Earth-facing and anti-Earth-facing sides. The equinox orbit pointing error in the east-west direction of the 7.5-m PMR for this analysis case (fig. 11) ranged from -40 to 30 arcseconds. Although these results approach the specified pointing requirements, for a few analysis points in the orbit, they do remain outside the specified limit.

Thermal blanket. A thermal blanket is an insulating technique that wraps the entire box truss with an aluminized Kapton sheet. The blanket radiatively decouples the truss structure from the orbital environment and eliminates internal shadowing,

thereby greatly reducing the uneven distributions in the absorbed and emitted radiative heat fluxes. This eliminates the large temperature difference between Earth-facing and anti-Earth-facing sides of the structure which, as the baseline analysis showed, is the primary cause of large east-west pointing errors. An analysis of the thermal blanket insulating technique resulted in pointing errors that were well within the required limits. Two analytical iterations were undertaken. The first iteration used surface properties of uncoated graphite for the truss beams and the inner side of the thermal blanket and a surface coating with an α/ϵ ratio of 0.3/0.2 on the outside of the blanket. Pointing performance was excellent, with a maximum east-west pointing error of -8 arcseconds for the 7.5-m PMR. However, because the ratio of absorptivity to emissivity of the outside surface was greater than unity, the absorbed solar radiation dominated the heat balance and the maximum temperature of the thermal blanket exceeded 110°C, which is beyond the material limits of Kapton.

The second iteration of the thermal blanket design employed an uncoated-graphite surface on the truss beams, a low α/ϵ ratio (0.3/0.65) surface coating on the outside surface of the blanket, and a low-emissivity (0.2) coating on the inside surface. The high-emissivity outside surface was very effective in increasing the emitted radiation, and the low-emissivity coating on the inside surface decreased the amount of heat radiated to the truss from the blanket. Using this configuration reduced the maximum blanket temperature to within the material limits of the Kapton without adversely affecting the east-west pointing error by a significant amount. At equinox, the minimum and maximum truss member temperatures are -114°C and -39°C, respectively. Figure 12 shows average element temperature as a function of time in equinox orbit for Earth-facing and anti-Earth-facing longerons of this thermal blanket configuration. Of particular interest is the excellent temperature tracking, indicating reduced temperature gradients and resulting in smaller pointing errors.

In the equinox orbit the east-west pointing error of the 15-m PMR ranges from 6 to 2 arcseconds and that of the 7.5-m PMR ranges from -14 to 3 arcseconds. Figure 13 shows the pointing errors of the 15-m and 7.5-m PMR's as a function of time in equinox orbit relative to the baseline pointing errors and illustrates the tremendous smoothing effect that the thermal blanket has on pointing error by eliminating internal shadowing. The solstice orbit exhibits similarly small east-west pointing errors ranging from 2 to 5 arcseconds for the 15-m PMR and from -10 to -2 arcseconds for the 7.5-m PMR. The improvement in the solstice orbit results compared with those of the baseline configuration further illustrates the advantageous effect of thermally decoupling the structure from the orbital environment.

Trends in Analytical Results

In the previous section the analytical results of the baseline configuration were presented. The results of each thermal enhancement were presented in terms of its capability to improve the thermal performance relative to the baseline configuration. The general trends in performance improvement will now be demonstrated by comparing the analyzed baseline configuration (case 1), the MLI sleeving configuration (case 4), and the final thermal blanket configuration (case 6). Specifically, the trends will be identified with regard to truss temperature and pointing error profiles. For brevity in describing the trends, the configurations will be identified by their case number as defined in table II. The three cases listed above were chosen because the analytical results of the MLI sleeving configuration and the final thermal blanket configuration show with clarity the amount of improvement in thermal performance that is attainable by applying those enhancement techniques to the baseline configuration. The two surface-coated configurations are eliminated from this discussion because of their relative ineffectiveness in improving the thermal performance.

Figure 14 shows the orbital variation in the minimum and maximum truss member temperatures for cases 1, 4, and 6 identified above and illustrates several points of interest. The most striking aspect shown by the curves is that cases 1 and 4 have nearly constant maximum and minimum temperatures, except for the coincident drops in the maximum temperature during the Earth's shadow, whereas the curves for case 6 track each other with a nearly sinusoidal shape. As stated previously, the maximum temperature correlates to a truss member that is exposed to direct solar flux, and the minimum temperature correlates to a truss member that is completely shadowed. In cases 1 and 4 there are truss members that are exposed and/or shadowed for all times of the orbit, excluding those in the Earth's shadow, and therefore exhibit the extreme temperatures consistently. In case 6, however, the thermal blanket shields all truss members from direct viewing of the solar flux and deep space, thereby acting as a buffer between the orbital environment and the truss. In addition, as the outside surface of the blanket on one side of the truss heats up from direct solar flux exposure, the inside surface radiates thermal energy to all internal blanket faces and truss members.

The result of this reradiating effect is a more uniform distribution of heat fluxes throughout the truss structure and, hence, much less of a difference between the maximum and minimum temperatures.

Also evident in figure 14 is that the difference between the minimum and maximum temperatures is greater for case 1. However, the maximum temperature curve for case 4 nearly traces that of case 1. The ratio of solar absorptivity to thermal emissivity (α/ϵ) induces this behavior by governing the ratio of incident solar energy absorbed to thermal energy emitted by those truss members that are exposed to the Sun. Because case 1 has an α/ϵ ratio of 1.125 and case 4 has an α/ϵ ratio of 1.0, the maximum temperatures are relatively close. In addition, case 4 has a significantly higher minimum temperature than case 1. The considerably lower thermal emissivity of case 4 causes the truss members not exposed to the Sun to retain much more thermal energy than those in case 1, thereby maintaining higher minimum temperatures. The temperature differences between the longerons of opposing sides of the truss structure, caused by internal shadowing, have been shown to be the primary cause of east-west pointing error in the equinox orbit. The trends in how the performance enhancements affect these temperature differences are of interest.

Figure 15 illustrates the orbital variation in the average temperature differences for the three cases described above. The maximum temperature difference between opposing longerons exceeds 170°C for case 1. The temperature difference is greatly reduced to around 75°C for case 4, and, again, significantly to below 10°C for case 6. The fundamental reasons for the reduced temperature differences are the same as those discussed above. Also apparent in figure 15 is the drop in the temperature difference around local midnight, when the entire structure is in the Earth's shadow and, therefore, when all truss members have a common radiative heat sink.

Figure 16 compares the worst-case pointing errors for cases 1, 4, and 6. By placing both of the performance enhancement cases on the same scale as the baseline configuration case, the relative amounts of pointing improvement that are achievable by applying the respective insulating techniques become more apparent.

Concluding Remarks

A thermal analysis of the main box truss structure of a geostationary platform concept was made. Structural element temperatures were obtained from a finite-difference analysis for positions throughout the geostationary orbit and were used to create the thermal loads for finite-element structural analysis. Thermal and structural analyses were made for equinox and solstice orbits. Performance results of the structural analysis were in terms of east-west and north-south pointing errors at the mounting locations of the two radiometers.

The baseline configuration employs an uncoated graphite/epoxy composite box truss construction. This material, although not practical because of the effects of the space environment on uncoated composite materials, serves to demonstrate typical thermal behaviors for this type of truss in a geostationary orbit. Also, the baseline configuration allows quantification of worst-case thermal distortions to which the performance of alternative thermal design options can be compared.

The worst thermal distortions for the baseline configuration led to significant east-west pointing errors during the equinox orbit. These east-west pointing errors resulted primarily from temperature differences between the Earth-facing and anti-Earth-facing truss longerons. The symmetrical design of the main box truss, combined with 0° declination at equinox, causes significant internal shadowing of longerons on the anti-Sun side, thereby greatly diminishing the solar heating on that side. The maximum east-west pointing errors for the 15-m and 7.5-m passive microwave radiometers (PMR's) were 25/-15 and 71/-99 arcseconds, respectively. The 7.5-m PMR fails to meet the required pointing accuracy of 36 arcseconds. Therefore, significant differences in temperature and distortions exist between the two sides. In the solstice orbit analyzed, the incident Sun angle of 23.5° eliminated the excessive internal shadowing of the longerons that was present in the equinox orbit, thereby greatly reducing the temperature differences between the opposing sides and the resulting east-west pointing errors. There is a proportionality of the pointing errors of the 7.5-m and 15-m PMR's to their distance from the restrained housekeeping and payload (H/P) modules.

Calculated north-south pointing errors are small relative to the east-west pointing errors and, unlike the east-west errors, marginally satisfy the specified pointing requirements for all configurations analyzed. The primary causes of the north-south pointing errors are unbalanced torsion effects induced by the thermal distortion of truss diagonals and batons. The imbalances are due to the truss lattice pattern and the odd number of bays on each side of the restrained module. Many configuration design changes exist that would greatly reduce or eliminate the north-south pointing errors, each of which requires further study to determine the impact on other features of the spacecraft design.

The thermal control options considered include surface coatings and insulating techniques and are evaluated relative to the baseline configuration with respect to their effectiveness in reducing the east-west pointing errors. The application of state-of-the-art surface coatings to the truss members decreases the pointing error by providing more favorable energy balances. However, the resulting reduced distortions remain above the specified error limits. An insulating technique that wraps individual truss elements with multilayer insulation (MLI) results in a significant improvement in pointing performance. However, the east-west pointing errors remain in excess of the specified error limits during certain portions of the equinox orbits. An insulating technique that encloses the entire truss within a thermal blanket of aluminized Kapton sufficiently decreases pointing errors such that the specified pointing requirements are satisfied. However, this approach may increase the complexity of deployment and/or erection as compared with the material coating or MLI-wrapped approaches.

These results indicate that improved pointing accuracy is achieved using several methods. However, only those methods that reduce radiative heat exchanges between the truss structure and the orbital environment and those that foster uniform distribution of the radiative fluxes throughout the truss structure are effective in reducing pointing error sufficiently to meet the specified pointing requirements of this mission. The thermal blanket configuration presented in this study was successful in meeting the specified pointing requirements for the 7.5-m and 15-m PMR's. However, the complexity that the thermal blanket adds to the deployment and/or erection scenario enlisted for this geostationary concept must be considered. Other techniques intended to achieve mission pointing requirements may be worthy of study, such as an asymmetrical truss design that precludes the occurrence of excessive internal shadowing under any possible orbital conditions. Again, modifications to the box truss design unavoidably require examination of their impact on other design features and characteristics. Another option that can be implemented for any configuration is to incorporate active on-orbit pointing corrections based on the predicted pointing errors. In order to fairly evaluate the techniques available for thermal performance enhancement, it is necessary to consider more issues than simply the expected thermal performance of each option. For example, the on-orbit handling, maintenance, complexity, and lifetime must be compared to the thermal performance gain anticipated.

NASA Langley Research Center
Hampton, VA 23665-5225
August 23, 1990

Appendix

Modeling and Analysis Tools

The structural and thermal analyses were performed using a system of computer-aided engineering software. This software includes Supertab (for visual inspection and modification of finite-element models and postprocessing of results), Thermal Model Generator (TMG) (for thermal modeling and analysis), and Model Solution (for linear, static structural analysis). A brief discussion of these tools follows, as addressed in reference 2.

Supertab

Supertab is part of the I-DEAS software system developed by the Structural Dynamics Research Corporation (SDRC). It is used to interactively build, visualize, and modify finite-element models prior to structural analysis and to visually interrogate the results of such an analysis. These models are analyzed in TMG or Model Solution, as discussed below; the results (such as temperatures, deflections, and stresses) are automatically translated back to Supertab for postprocessing.

Thermal Model Generator

TMG is an integrated thermal analysis tool developed by MAYA Heat Transfer Technologies Ltd. of Canada that works in conjunction with SDRC's Supertab to perform complete thermal modeling and analysis tasks. More specifically, TMG accepts the finite-element geometric model output from Supertab and employs an interactive menu-driven input system to build a complete lumped-parameter (or finite-difference) thermal model that can be used to estimate steady-state or transient element temperatures for subsequent thermal-structural analysis.

In building this thermal model, TMG performs several intermediate functions: it translates finite-element model data into a surface model for calculation of radiation heat transfer characteristics and into a finite-difference thermal network model by calculating conductive conductances and thermal capacitances; it calculates radiation exchange view factors, radiative conductances, and orbital heat fluxes (including the effects of shadows and reflections) using techniques based on diffuse enclosure assumptions; it uses these radiative couplings and heat fluxes along with the translated finite-difference model to calculate steady-state or transient temperature distributions and heat transfer rates employing thermal network techniques and various matrix solution algorithms; it maps these temperatures back onto the finite-element model and translates them into Supertab for graphical postprocessing and as input to Model Solution. TMG performs these functions in an integrated nature, thus automating the entire process.

Model Solution

Model Solution is the primary numerical solver for the I-DEAS software package. Its direct connection with Supertab significantly automates modeling, analysis, and visualization of results. Its linear static structural analysis capability used for this study is based on a finite-element formulation of linearized structural deformation equations. Inputs include the finite-element model built in Supertab, a restraint set or boundary conditions, and the element temperatures that act to produce structural loads. Model Solution estimates the displacements of the nodes in the finite-element model of the reflector strongback as well as element stresses caused by these loads and translates them back to Supertab where they can be graphically examined.

References

1. Wahls, Deborah M.; Farmer, Jeffery T.; and Sleight, David W.: *On-Orbit Structural Dynamic Performance of a 15-Meter Microwave Radiometer Antenna.* NASA TP-3041, 1990.
2. Farmer, Jeffery T.; Wahls, Deborah M.; and Wright, Robert L.: *Thermal-Distortion Analysis of an Antenna Strongback for Geostationary High-Frequency Microwave Applications.* NASA TP-3016, 1990.
3. *Supertab—Engineering Analysis Pre- and Post-Processing User Guide.* I-DEAS Level 4, Structural Dynamics Research Corp., 1988.
4. *TMG—Thermal Model Generator—A Thermal Analysis Computer Program (TMG User's Manual).* Revision 2.2, MAYA Heat Transfer Technologies Ltd., Montreal, Canada, 1988.
5. *Supertab—Engineering Analysis Model Solution and Optimization User Guide.* I-DEAS Level 4, Structural Dynamics Research Corp., 1988.
6. Pidgeon, David Joseph: A Subsystem Design Study of an Earth Sciences Geostationary Platform. M.S. Thesis, The George Washington University, 1989.
7. Agrawal, Brij N.: *Design of Geosynchronous Spacecraft.* Prentice-Hall, Inc., c.1986.
8. Hedgepeth, John M.: Accuracy Potentials for Large Space Antenna Reflectors With Passive Structure. *J. Spacecr. & Rockets*, vol. 19, no. 3, May–June 1982, pp. 211–217. (Also available as AIAA-82-4136.)
9. Dursch, H.; and Hendricks, C.: *Development of Composite Tube Protective Coatings.* NASA CR-178116, 1986.

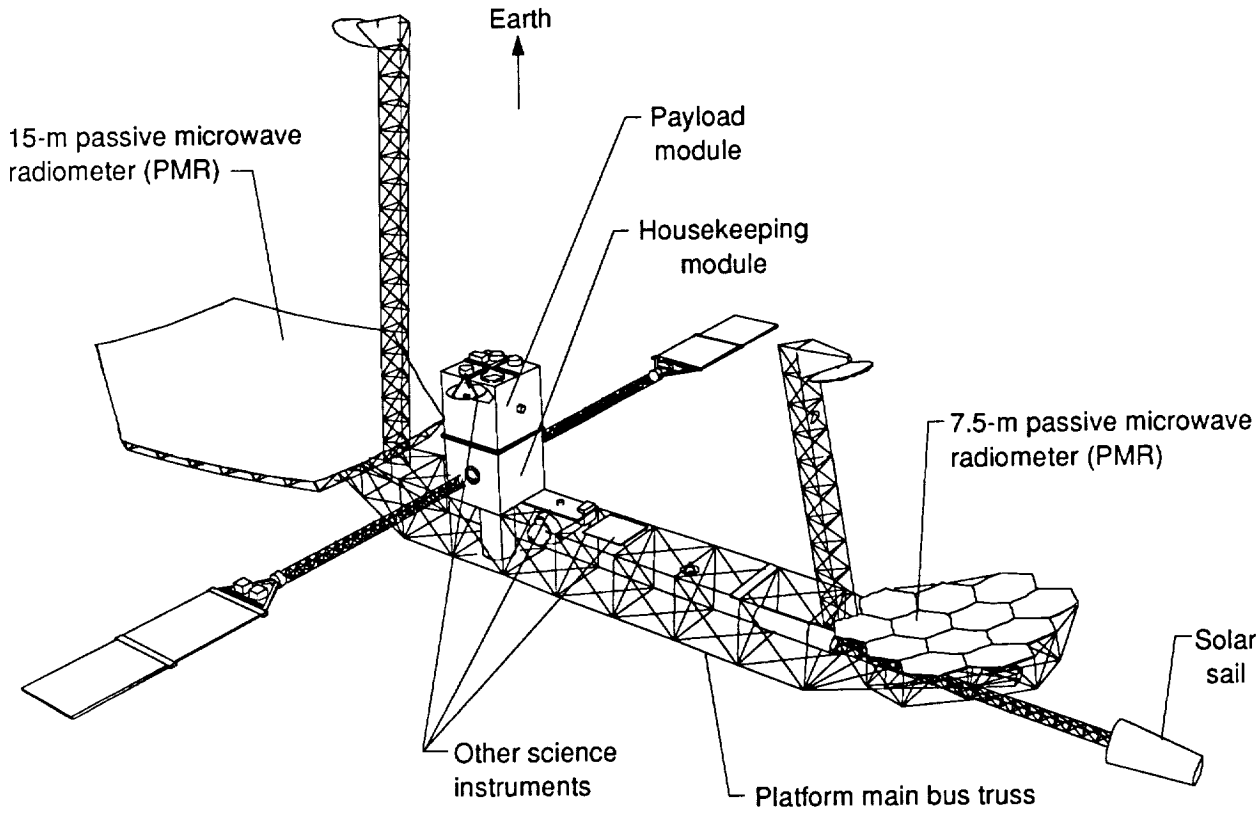

Figure 1. Geostationary Earth-science platform.

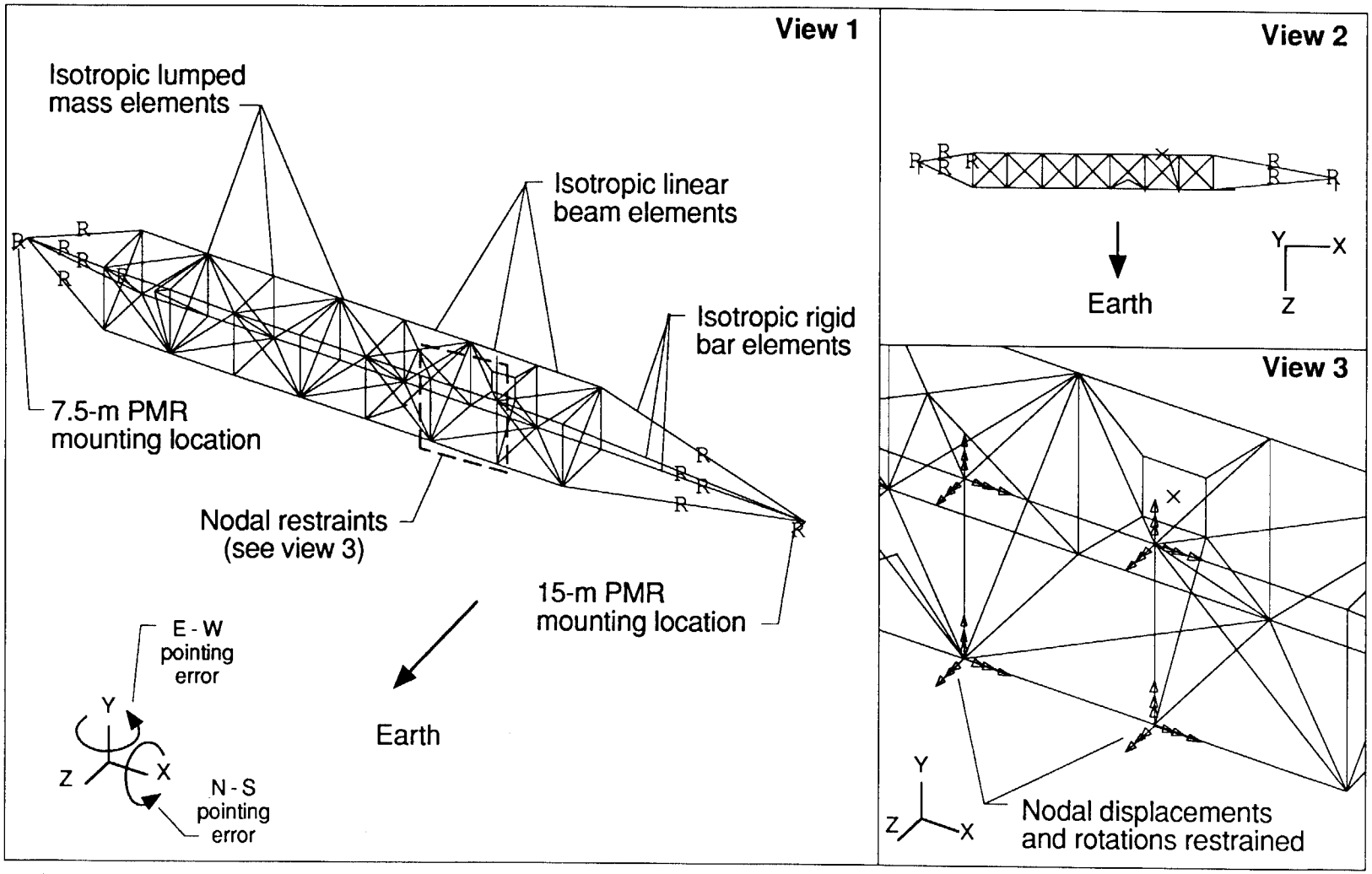

Figure 2. Finite-element model of bus truss.

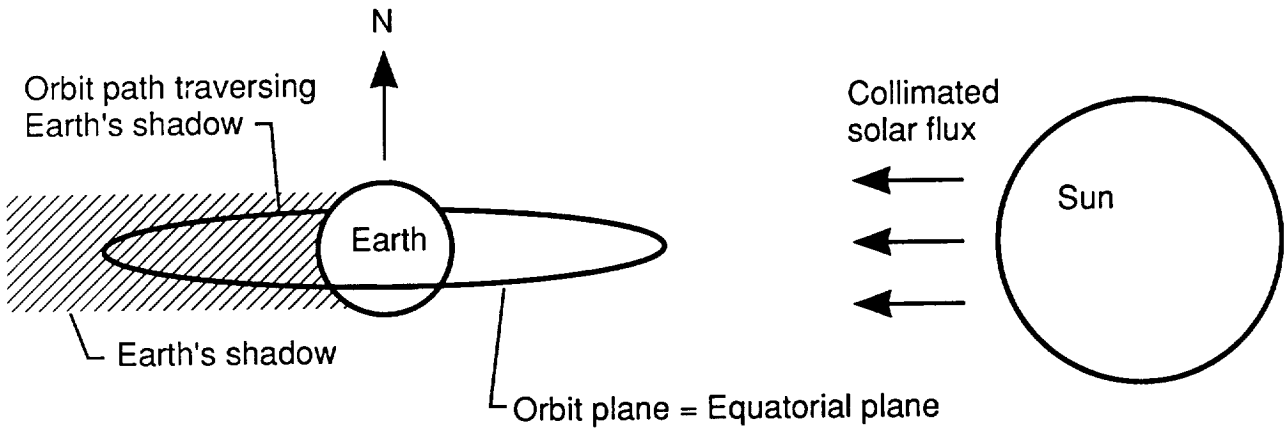

(a) Equinox orientation.

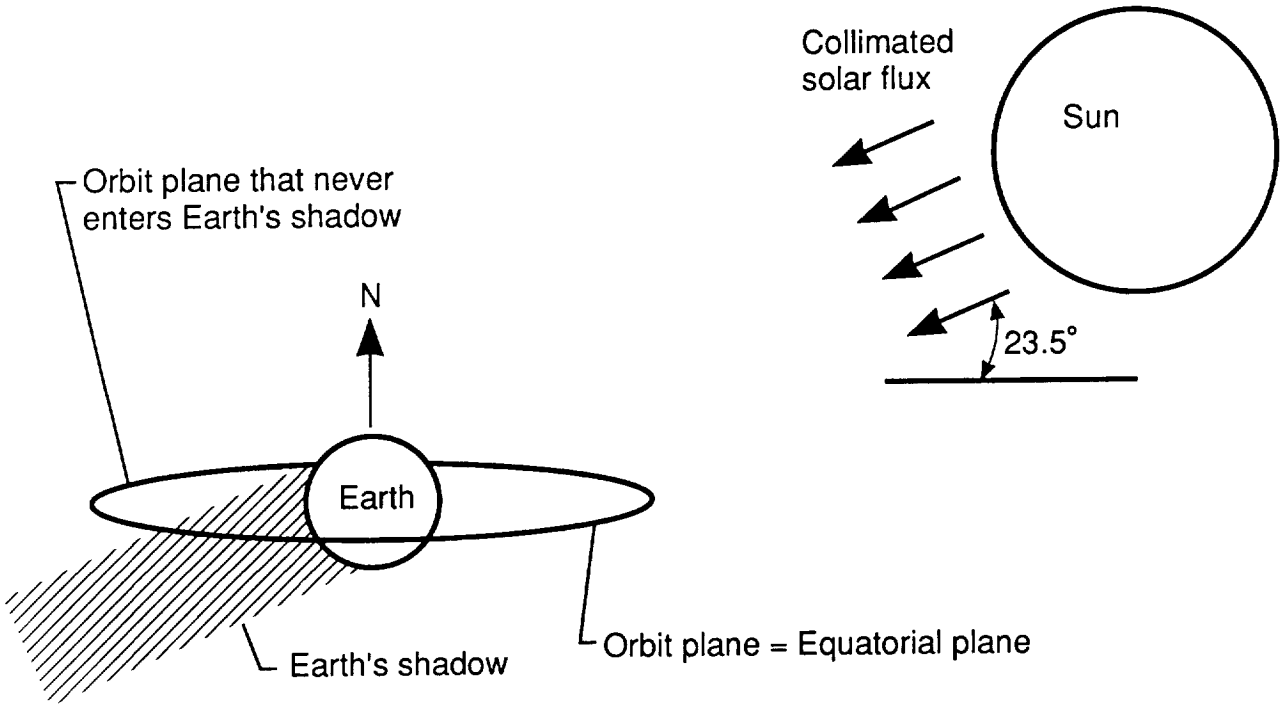

(b) Summer solstice orientation.

Figure 3. Earth's shadow at equinox and solstice.

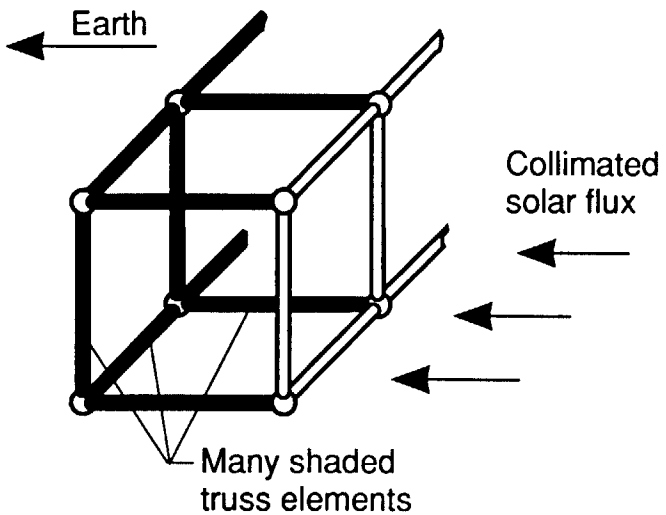

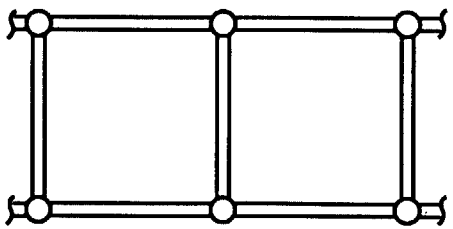

Since projected areas of Earth-facing and anti-Earth-facing sides are coincident, there is extensive internal shadowing. Viewed from plane of incident solar flux.

(a) Equinox orientation.

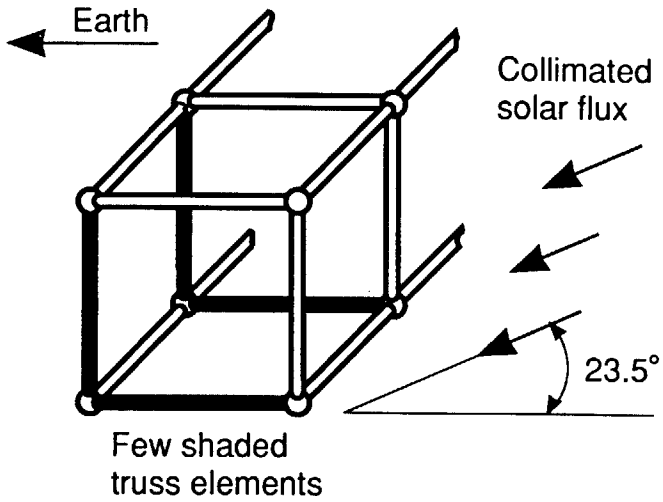

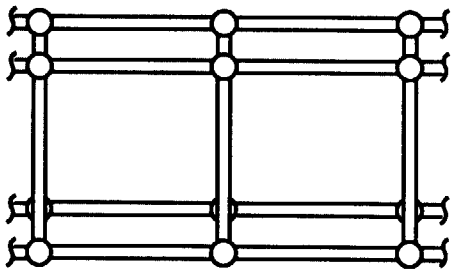

Since projected areas of Earth-facing and anti-Earth-facing sides are not coincident, there is reduced internal shadowing. Viewed from plane of incident solar flux.

(b) Solstice orientation.

Figure 4. Views at solar noon.

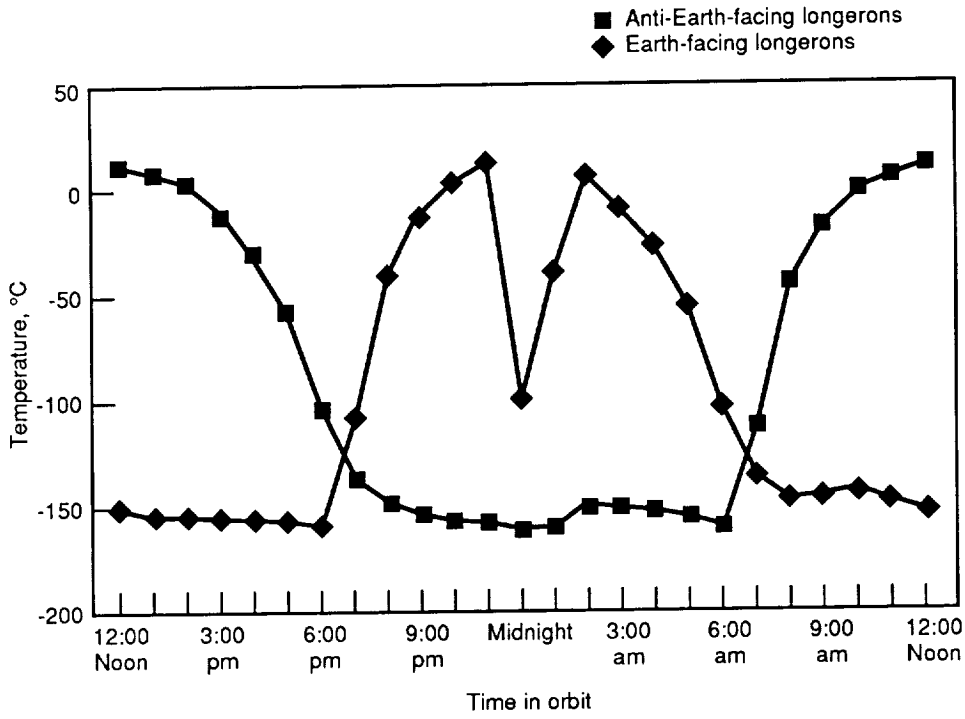

Figure 5. Orbital variation of average temperatures of longerons for baseline configuration in equinox orbit.

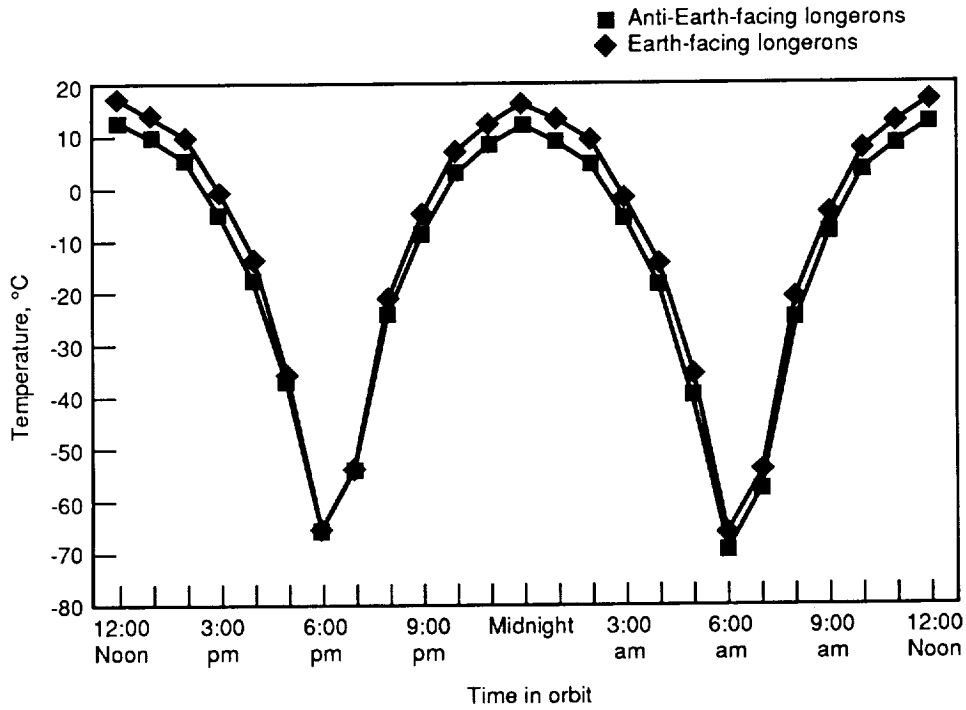

Figure 6. Orbital variation of average temperatures of longerons for baseline configuration in solstice orbit.

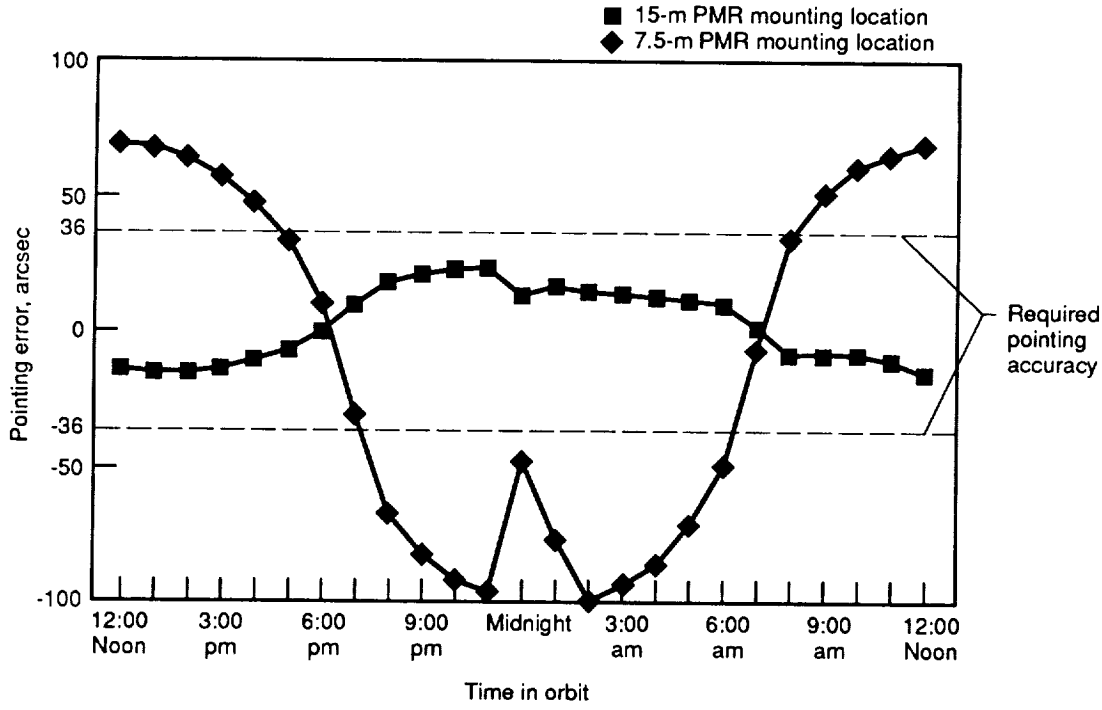

Figure 7. East-west pointing error at PMR mounting locations as a function of equinox orbital position.

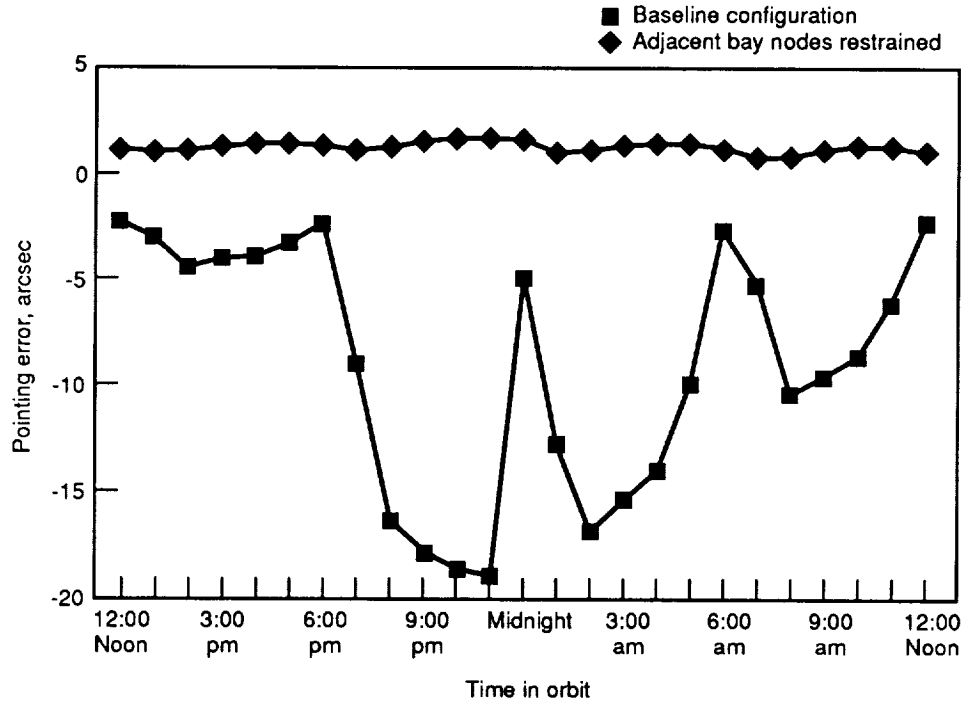

Figure 8. Comparison of north-south pointing error of 7.5-m PMR with nodal restraints added to baseline configuration in equinox orbit.

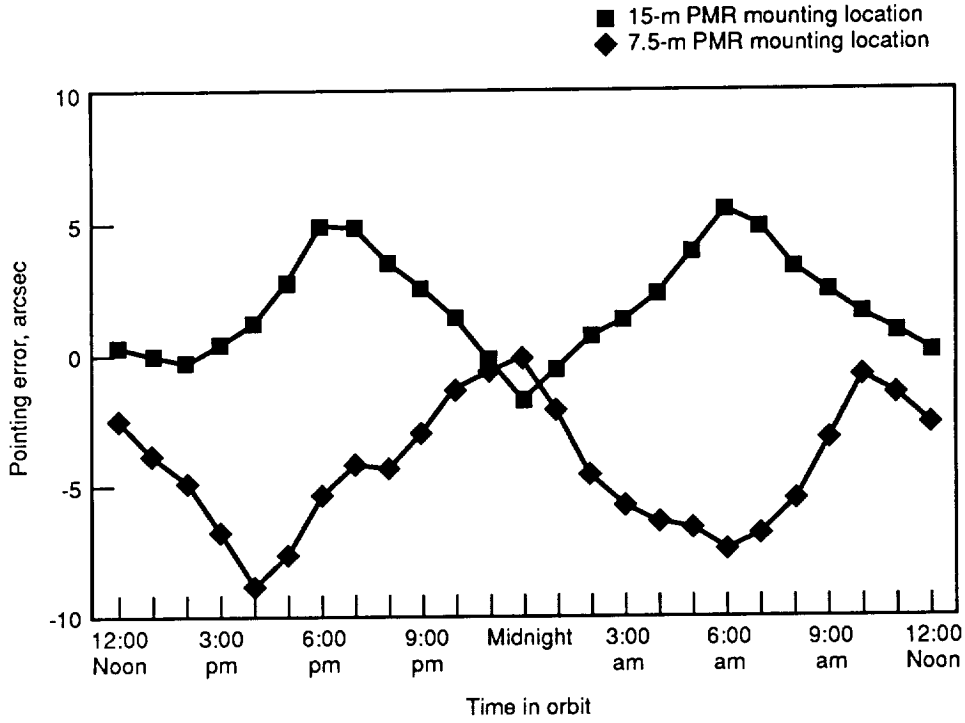

Figure 9. East-west pointing error at PMR mounting locations for baseline configuration in solstice orbit.

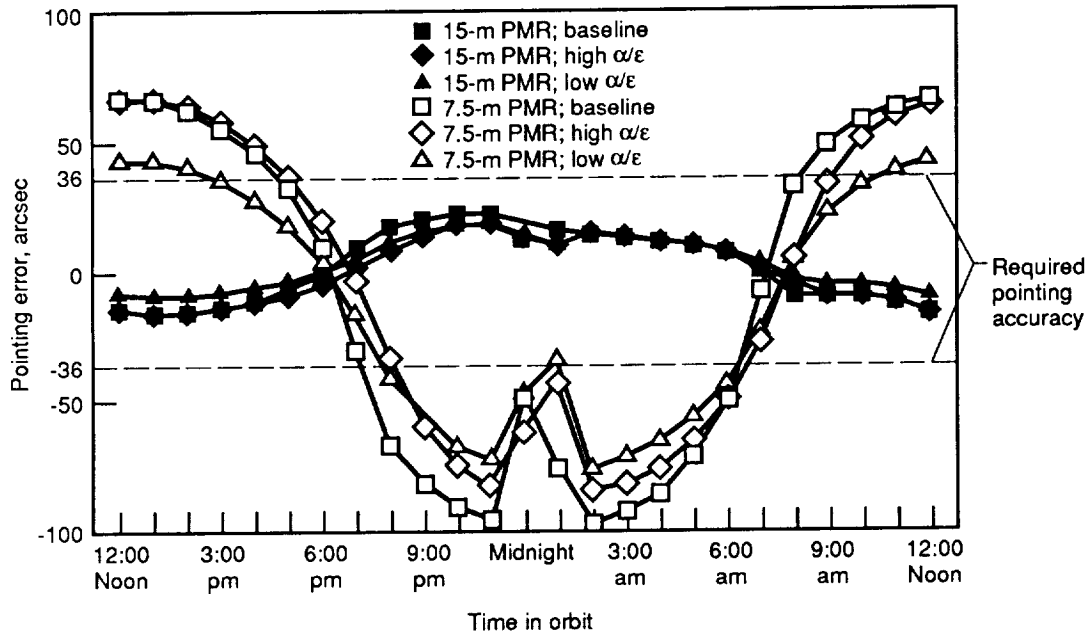

Figure 10. Comparison of baseline configuration and surface-coating cases for east-west pointing error in equinox orbit.

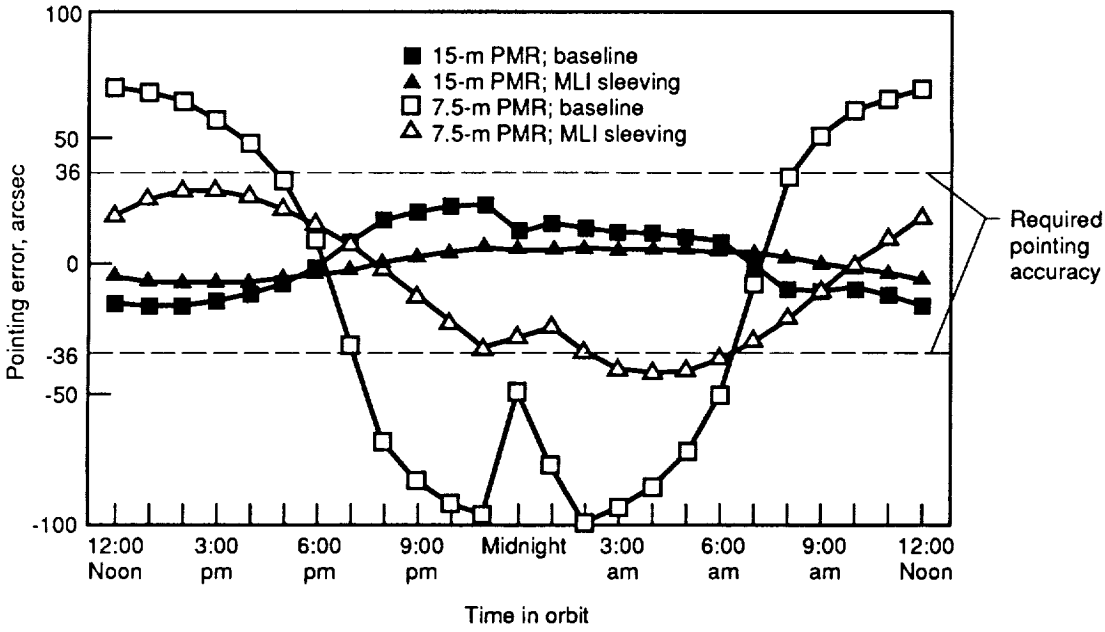

Figure 11. Comparison of baseline configuration and MLI sleeving case for east-west pointing error in equinox orbit.

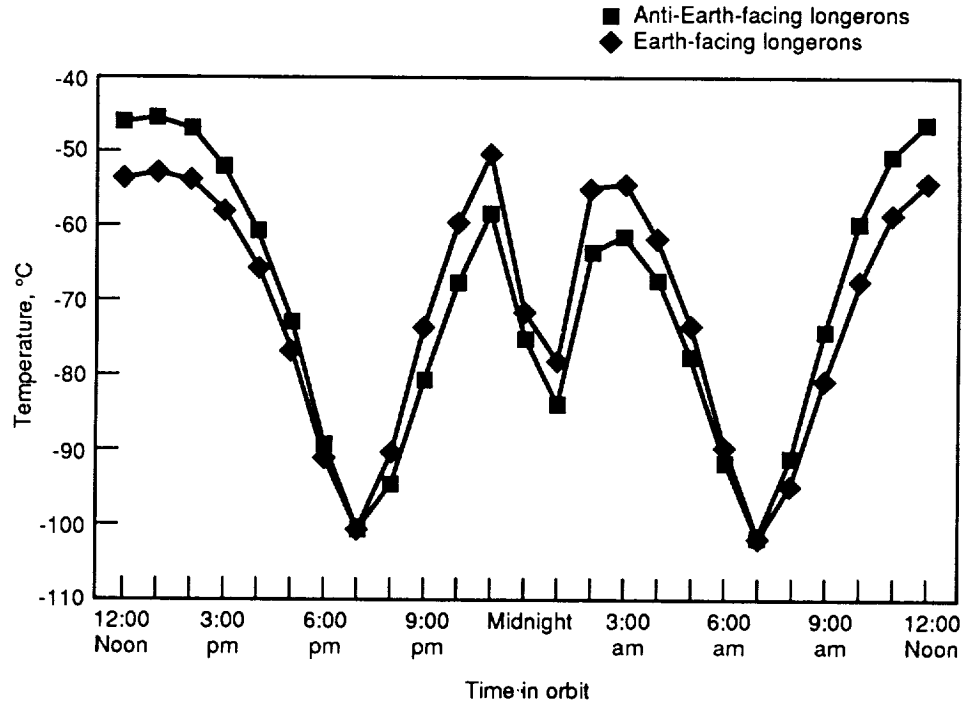

Figure 12. Orbital variation of average temperatures of longerons for final thermal blanket case in equinox orbit.

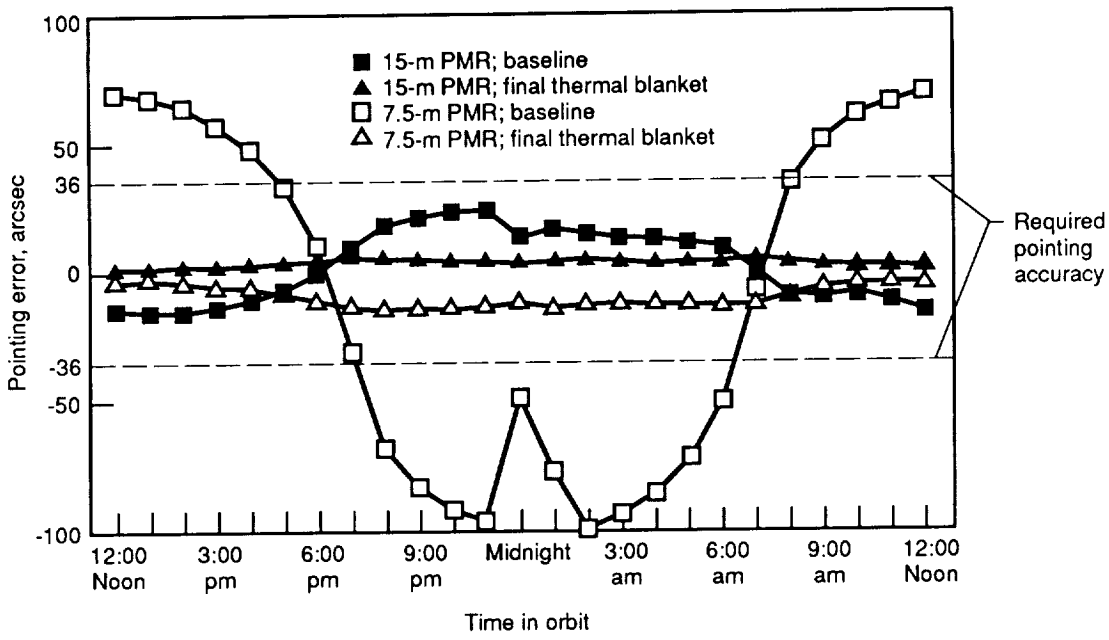

Figure 13. Comparison of baseline configuration and final thermal blanket case for east-west pointing error in equinox orbit.

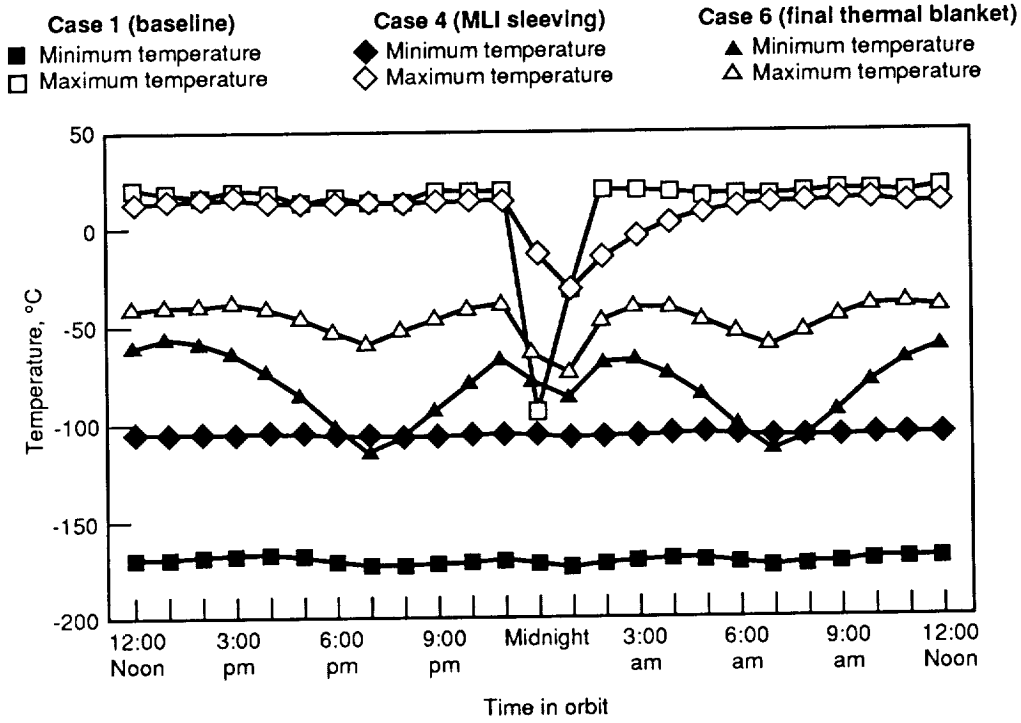

Figure 14. Orbital variation in minimum and maximum truss beam temperatures for three cases in equinox orbit.

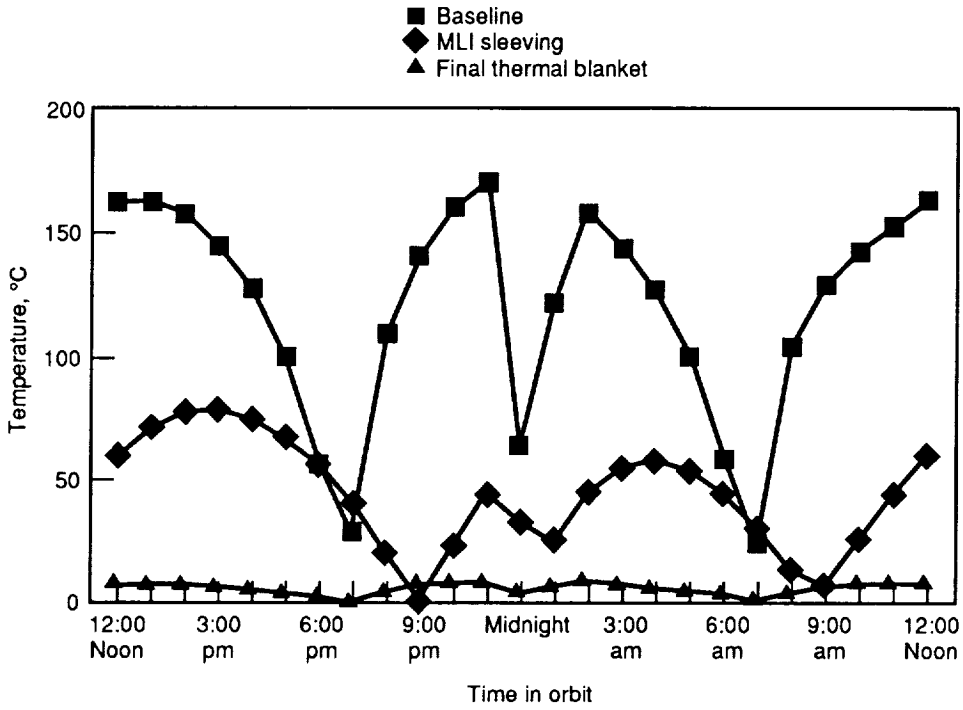

Figure 15. Orbital variation of average temperature difference between Earth-facing and anti-Earth-facing longerons for three cases in equinox orbit.

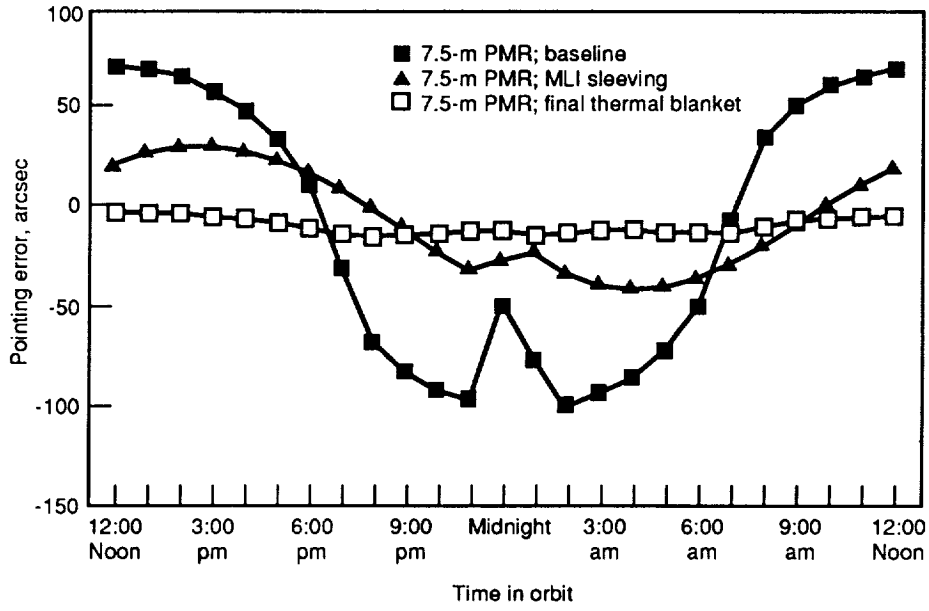

Figure 16. Comparison of east-west pointing errors at 7.5-m PMR mounting locations for three cases in equinox orbit.

NASA
National Aeronautics and Space Administration

Report Documentation Page

1. Report No.	2. Government Accession No.	3. Recipient's Catalog No.
NASA TP-3054		

4. Title and Subtitle	5. Report Date
Thermal-Distortion Analysis of a Spacecraft Box Truss in Geostationary Orbit	November 1990
	6. Performing Organization Code
7. Author(s)	8. Performing Organization Report No.
Patrick A. Cosgrove, Jeffery T. Farmer, and Lawrence F. Rowell	L-16828
9. Performing Organization Name and Address	10. Work Unit No.
NASA Langley Research Center Hampton, VA 23665-5225	506-49-21-02
	11. Contract or Grant No.
12. Sponsoring Agency Name and Address	13. Type of Report and Period Covered
National Aeronautics and Space Administration Washington, DC 20546-0001	Technical Paper
	14. Sponsoring Agency Code

15. Supplementary Notes

Patrick A. Cosgrove: Lockheed Engineering & Sciences Company, Hampton, Virginia.
Jeffery T. Farmer and Lawrence F. Rowell: Langley Research Center, Hampton, Virginia.

16. Abstract

The Mission to Planet Earth program may enlist the use of geostationary platforms to support Earth-science monitoring instruments. The strongback for a proposed geostationary platform is a deployable box truss that supports two large-diameter passive microwave radiometers (PMR's) and several other science instruments. A study was made to estimate the north-south and east-west pointing errors at the mounting locations of the two PMR's due to on-orbit thermal distortions of the main truss. The baseline configuration for the main truss was modeled as untreated graphite/epoxy composite truss members and end fittings to illustrate typical thermal behaviors for structures of this type. Analytical results of the baseline configuration indicated that the east-west pointing error greatly exceeded the required limits. Primary origins of the pointing errors were identified, and methods for their reduction were addressed. Thermal performance enhancements to the truss structure were modeled and analyzed, including state-of-the-art surface coatings and insulation techniques. Comparisons of the thermal enhancements to the baseline were made. Results demonstrated that using a thermal-enclosure insulating technique reduced external heat fluxes and distributed those heat fluxes more evenly throughout the structure, sufficiently reducing the pointing errors induced by thermal distortions to satisfy pointing accuracy requirements of the PMR's.

17. Key Words (Suggested by Authors(s))	18. Distribution Statement
Thermal-distortion analysis Spacecraft main box truss Geostationary orbit Induced pointing error	Unclassified—Unlimited Subject Category 18

19. Security Classif. (of this report)	20. Security Classif. (of this page)	21. No. of Pages	22. Price
Unclassified	Unclassified	23	A03

NASA FORM 1626 OCT 86

NASA-Langley, 1990

For sale by the National Technical Information Service, Springfield, Virginia 22161-2171

National Aeronautics and
Space Administration
Code NTT-4

Washington, D.C.
20546-0001